JOURNAL OF GEOPHYSICAL RESEARCH, VOL. 113, A10304, doi:10.1029/2008JA013490, 2008

Topside ionospheric scale heights retrieved from Constellation Observing System for Meteorology, Ionosphere, and Climate radio occultation measurements

Libo Liu,[1] Maosheng He,[1] Weixing Wan,[1] and Man-Lian Zhang[1]

Received 13 June 2008; revised 9 July 2008; accepted 24 July 2008; published 11 October 2008.

[1] The vertical scale height (VSH) in the topside ionosphere can be derived from electron density profiles. In this study, the electron density profiles retrieved from the COSMIC/FORMOSAT-3 (a Constellation Observing System for Meteorology, Ionosphere, and Climate mission; C/F3 for short) ionospheric radio occultation (IRO) observations have been collected to investigate the local time, seasonal, latitudinal, and longitudinal variations of the VSH. With the postprocessed C/F3 IRO electron density profiles during the interval from day of year (DOY) 194 in 2006 to DOY 60 in 2008, we conduct an analysis on the behaviors of VSH at an altitude of 400 km. There are appreciable latitudinal variations in VSH. A new finding is a significant peak around dip equator during daytime in four seasons. Away from the equatorial peak, it is obvious that the VSH generally increases at higher latitudes. The equatorial VSH undergoes a significant diurnal variation with a local noon maximum. The peak shifts to sunrise time with increasing dip latitude, and the values of daytime VSH become comparable with those at nighttime at low latitude in both hemispheres, which is somewhat different from the feature revealed from Arecibo incoherent scatter radar observations. One of the crucial findings in our results is the most outstanding feature of VSH, that is, the presence of a substantial longitudinal structure in equatorial regions. A wave-like longitudinal feature is found in equatorial VSH during the daytime in four seasons, while it becomes weaker or absent at other local time intervals and at higher latitudes. This investigation also confirms that the behaviors of VSH are not strongly consistent with those of the neutral or plasma-scale heights.

Citation: Liu, L., M. He, W. Wan, and M.-L. Zhang (2008), Topside ionospheric scale heights retrieved from Constellation Observing System for Meteorology, Ionosphere, and Climate radio occultation measurements, *J. Geophys. Res.*, *113*, A10304, doi:10.1029/2008JA013490.

1. Introduction

[2] The spatial distribution of electron densities (N_e) in the ionosphere, especially the height profile $N_e(h)$, provides key information for ionospheric scientific studies as well as for associated practical applications. For many years, several mathematical functions, such as Chapman, exponential, parabolic, and Epstein functions, have been proposed to estimate the ionospheric height profiles [e.g., *Booker*, 1977; *Rawer et al.*, 1985; *Rawer*, 1988; *Di Giovanni and Radicella*, 1990; *Bilitza*, 2001; *Bilitza et al.*, 2006; *Stankov et al.*, 2003; *Reinisch et al.*, 2004; *Reinisch and Huang*, 2001]. An important and inherent parameter for these profile functions is the ionospheric scale height [*Huang and Reinisch*, 1996, 2001; *Stankov et al.*, 2003; *Belehaki et al.*, 2006]. The ionospheric scale heights measure the shape of electron density profile, indicates the gradient of electron density, and intrinsically connects to ionospheric dynamics, plasma temperature and compositions [e.g., *Luan et al.*, 2006; *Stankov and Jakowski*, 2006b; *Liu et al.*, 2007a, 2007b].

[3] It is interesting that topside modelings often rely on the vertical scale height (VSH) or the Chapman-scale height H_m, not directly on the standard plasma-scale height (H_p). The VSH is generally defined as $-dh/d(\ln(N_e))$ [e.g., *Kutiev et al.*, 2006; *Liu et al.*, 2007a, 2007b], the vertical distance in which the topside N_e changes by a factor of e (= 2.71828) under an assumption of a topside profile exponentially decaying with altitude. With this assumption, VSH can be approximately deduced from the gradient of a topside N_e profile in a least squares sense, as did in this report. In contrast, H_p is defined as $H_p = k_b T_p/m_i g$. Here k_b is Boltzmann's constant, g the acceleration due to gravity, m_i the ion mass, and $T_p = T_i + T_e$ is the plasma temperature (T_i, T_e the ion and electron temperatures). There are evidences that VSH might not be so tightly correlated with the plasma temperature T_p. Possible relationships between these ionospheric scale heights have been discussed by *Liu et al.*

[1]Beijing National Observatory of Space Environment, Institute of Geology and Geophysics, Chinese Academy of Sciences, Beijing, China.

0148-0227/08/2008JA013490$09.00

[2007a, 2007b], in which the sensitivity of ionospheric scale heights to thermal structure and dynamics is confirmed.

[4] During the past decades, several techniques, such as satellite in situ measurements, ground and topside ionosondes, and incoherent scatter radars, have been used for probing the structure of the ionosphere. With the developing of Global Navigation Satellite System, such as the Global Positioning System (GPS), ionospheric radio occultation (IRO) observations onboard on low Earth orbiting (LEO) satellites, become a powerful new technique to remotely sense the vertical and horizontal structure of the ionosphere with high data coverage on global scale. Some studies have shown promised IRO results in comparison with other measurements. The electron density profiles retrieved from IRO measurements onboard on LEO satellites, such as COSMIC/FORMOSAT-3 (a Constellation Observing System for Meteorology, Ionosphere, and Climate mission) [*Lei et al.*, 2007; *Lin et al.*, 2007; *Schreiner et al.*, 2007], CHAMP (Challenging Minisatellite Payload for Geophysical Research and Application) [e.g., *Jakowski et al.*, 2002; *Liu et al.*, 2007], SAC-C [*Hajj et al.*, 2004], and other missions, bring a new data resource for understanding global ionospheric structures and their behaviors.

[5] The VSH is frequently used in various practical applications. Electron density profiles measured from the techniques mentioned above have been used to retrieve topside-scale heights in the literature, which have provided significant contributions to the knowledge of ionospheric scale heights. For example, *Stankov and Jakowski* [2006a, 2006b] retrieved the topside ionospheric scale heights from 1 year radio occultation measurements onboard the CHAMP satellite; *Kutiev et al.* [2006] used topside ionosonde observations from Alouoette and ISIS satellites to develop a model of the topside ionosphere-scale height; and *Belehaki et al.* [2006] compared the ionosphere-scale heights retrieved from topside sounder profiles with those from a Digisonde at Athens. *Lei et al.* [2005] and *Liu et al.* [2007b] analyzed the Millstone Hill and Arecibo ISR observations to investigate the seasonal and solar activity features of the Chapman-scale height H_m. Subsequently, the morphology of H_m was statistically investigated in terms of ionosonde measurements at Wuhan (114.4°E, 30.6°N) by *Liu et al.* [2006], at Hainan (109.0°E, 19.4°N) by *Zhang et al.* [2006], at Jicamarca (76.9°W, 12°S) by *Lee and Reinisch* [2007], and at Grahamstown (26.5°E, 33.3°S) by *Nambala et al.* [2008].

[6] Knowledge of the behavior of scale heights in the topside ionosphere, however, still remains insufficient. For instance, very few studies have been made so far to determine the longitudinal variation of VSH although the longitudinal pattern of VSH is important for global modeling [*Depuev and Pulinets*, 2004]. This difficulty is partly due to the global observation insufficiency. Thus, it is an urgent issue to provide the global features of ionospheric scale heights. Fortunately, it is now available the accumulated IRO electron density profile databases, which provide an extremely valuable data source for addressing this issue.

[7] In this report, we collect the postprocessed COSMIC/FORMOSAT-3 (C/F3, for short) IRO electron density profiles during the interval from day of year (DOY) 194 in 2006 to DOY 60 in 2008 which are archived at UCAR (USA) to investigate the features of VSH. Approximately 1000–2600 occultation events per day were registered by C/F3. With the huge number of IRO electron density profiles, we conduct a statistical analysis on the diurnal and seasonal variations of VSH as well as its latitudinal and longitudinal distribution. The most significant feature of VSH in our results is the presence of a complicated longitudinal structure in equatorial regions, which is one of crucial findings of this analysis.

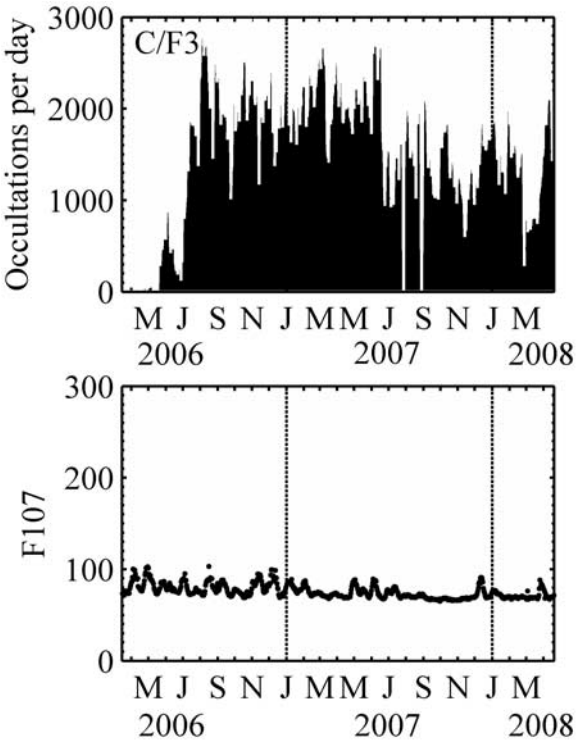

Figure 1. The COSMIC/FORMOSAT-3 IRO profile number and solar F10.7 flux.

2. Data Source and VSH Derivation

[8] The newly launched C/F3, a Constellation Observing System for Meteorology, Ionosphere, and Climate mission consisting of six satellites, measures GPS signals from which electron density profiles are derived with IRO techniques [e.g., *Rocken et al.*, 2000; *Lei et al.*, 2007; *Schreiner et al.*, 2007]. The inversion of electron density profiles is based on the assumption of local spherical symmetry of electron density. Although the local spherical symmetry may be a strong assumption and the horizontal structures may significantly affect the retrieved profiles in some cases, preliminary validations of the C/F3 IRO observations have been carried out by *Lei et al.* [2007] and *Schreiner et al.* [2007], which displayed good agreement with Jicamarca and Millstone Hill ISR and 31 globally distributed ionosonde measurements. This indicates that electron density profiles retrieved from C/F3 IRO observations can be used for ionospheric physics studies [*Lei et al.*, 2007]. The reader is referred to *Lei et al.* [2007], *Lin et al.* [2007], and *Schreiner et al.* [2007] for detail information on the C/F3 mission and IRO profile inversion technique.

[9] The electron density profiles collected for this investigation are the postprocessed C/F3 data, which are obtained

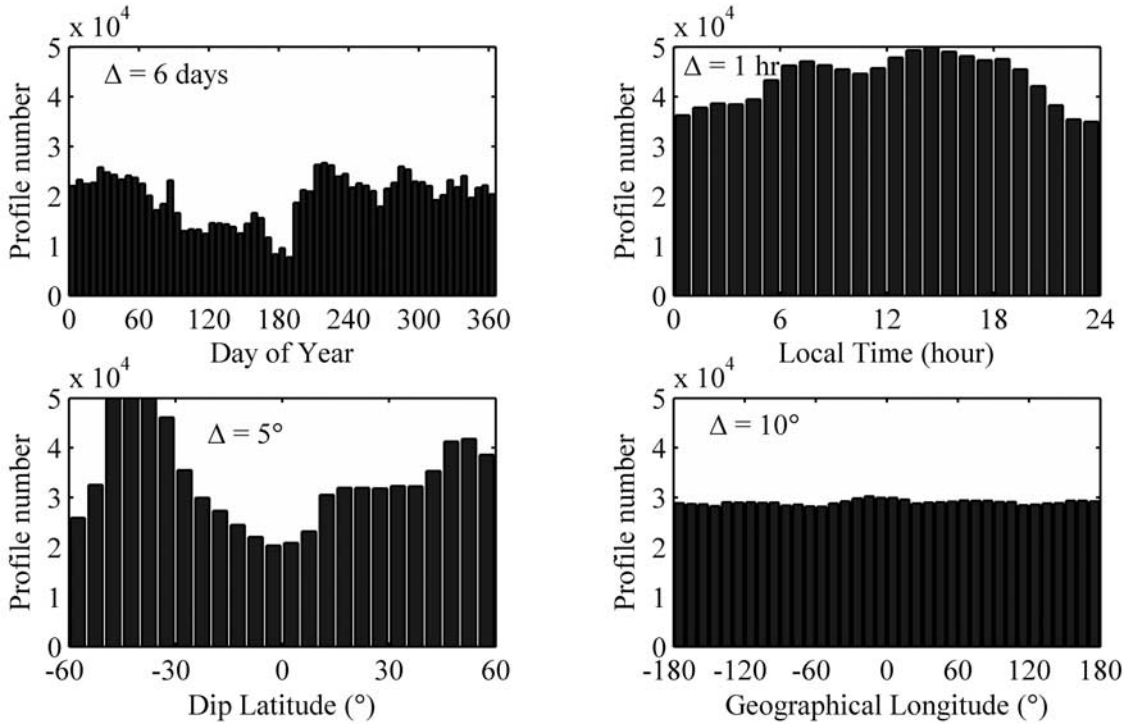

Figure 2. Profile distributions as function of day of year, local time, dip latitude, and longitude.

from the COSMIC Data Analysis and Archive Center (CDAAC). Figure 1 illustrates the daily profile numbers of IRO measurements and the variation of $F_{10.7}$. The 10.7 cm solar radio flux, $F_{10.7}$, is used as a standard proxy for solar activity. The $F_{10.7}$ index is provided at the SPIDR web site. The post processed C/F3 data are now available for the period from DOY 111 in 2006 to DOY 60 in 2008. While the data are posted starting on DOY 111 in 2006, we used the data starting on DOY 194 in 2006, according to a strong recommendation from the CDAAC team. During this period, the level of solar activity is at its minimum phase (Figure 1). The mean value of F10.7 is 76.6, while the daily values of F10.7 vary within a range from 65.1 to 103.2.

[10] First the IRO data have been checked for quality of retrieval. Then we fit each individual N_e profile within 160–600 km using a Chapman α function as described by *Lei et al.* [2005, 2007] and *Liu et al.* [2007a, 2007b]. The peak electron density (N_mF_2), its height (h_mF_2), and H_m are determined with a least squares fitting procedure. Good agreement prevails in most profiles, and we discard those profiles when significant deviations may occur under extreme conditions. It should be noted that retrieved electron density profiles should not be simply interpreted as actual vertical profiles, but rather as a mapping of both vertical and horizontal ionospheric structure into a one-dimensional profile, given a particular occultation geometry. Within the period from DOY 194 in 2006 to DOY 60 in 2008, more than 1,140,000 IRO events were recorded, and out of which about 1,000,000 electron profiles were obtained. After determining h_mF_2, the values of VSH in the topside ionosphere can be obtained from the slope of the lower topside N_e profiles with a least squares fitting. We just apply analysis on the profiles in the topside with altitudes starting several tens of kilometers above h_mF_2. The retrieved scale heights at different altitudes thereby should be an indicator of the shape of vertical electron density within the fitting region. The latitude and longitude corresponding to the VSH are also interpolated from the locations of the IRO profile.

[11] Figure 2 illustrates the distributions of the number of good quality profiles as function of DOY, local time, dip latitude, and longitude, indicating that the data is uniformly distributed in longitude and local time. There are 2 years data starting on DOY 194 in 2006, as a result, the number of profiles are much higher since DOY 194, compared to the first half part (DOY from 61 to 193). A gap of 2 months of FM6 and the power issues with FM2 and FM3 also cause the uneven data distribution in day of year. We can see that the C/F3 registered much larger IRO data, compared to previous IRO missions.

[12] Two example profiles of electron density as function of altitude on DOY 1 in 2007 are illustrated in Figure 3 (left) and the corresponding derived VSH in Figure 3 (right). From Figure 3, we can see that there are significant altitude variations of VSH. In this investigation, we restrict our attention to the behaviors of VSH at altitude of 400 km (We choose this altitude to make sure of that it lies at above the peak height of the F2 layer for most profiles.) In the following, VSH_{400} denotes the value of VSH at 400 km altitude.

3. Results

[13] Investigations have shown that the solar activity can affect the behavior of VSH [e.g., *Liu et al.*, 2007a]. In the present investigation, however, the solar activity is at its minimum phase (see Figure 1). Thus we can ignore the possible effect of solar activity on VSH in the following analysis without seriously affect the conclusion of our results.

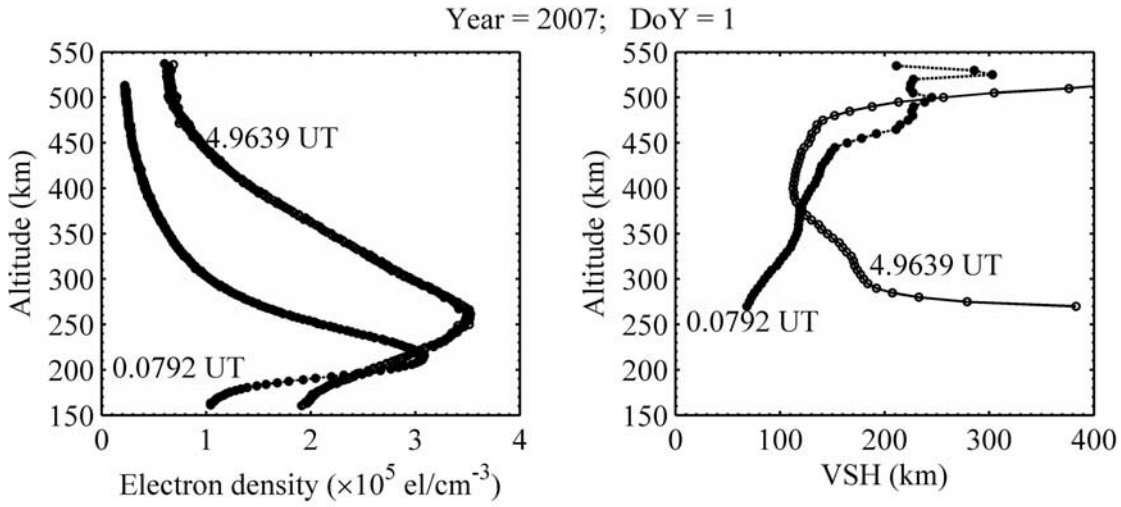

Figure 3. Two example profiles of (left) electron density and the (right) derived VSH on DOY 1 in 2007.

3.1. Local Time Variation of VSH

[14] Averaged values of VSH were obtained by binning VSH_{400} from 60 days (e.g., DOY [90–150] for vernal equinox) in every 3 h with moving windows, and taking median value of observations located in the given latitude grid. Figures 4a–4c plots VSH_{400} at dip equator (4°S–4°N dip latitude; Figure 4a), northern low latitude (19–25°N dip latitude; Figure 4b), and southern low latitude (19–25°S dip latitude; Figure 4c) as a function of local time in four seasons. Vertical bars in Figures 4a–4c depict the corresponding standard deviation values to show the scatter around the averages. The data points in each bin are plotted in the bottom of each part of Figures 4a–7d. From the data distribution, we can clearly find that the data sample sufficiently all parameter's range.

[15] In the equatorial region, as illustrated in Figure 4a, the VSH_{400} has distinct diurnal variations in four seasons. The values of equatorial VSH_{400} are higher during daytime, compared to those in the nighttime. There is a weak peak at 0400–0500 LT. Then VSH_{400} turns to descend. After approaching a minimum two hours later, the VSH value rises again, and an outstanding peak presents around local noon in four seasons. In the afternoon it decreases again till midnight.

[16] From Figures 4b and 4c, we can see that the diurnal variation of VSH_{400} at low latitudes is quite different from that in the equatorial region. A peak around 0600 LT can be

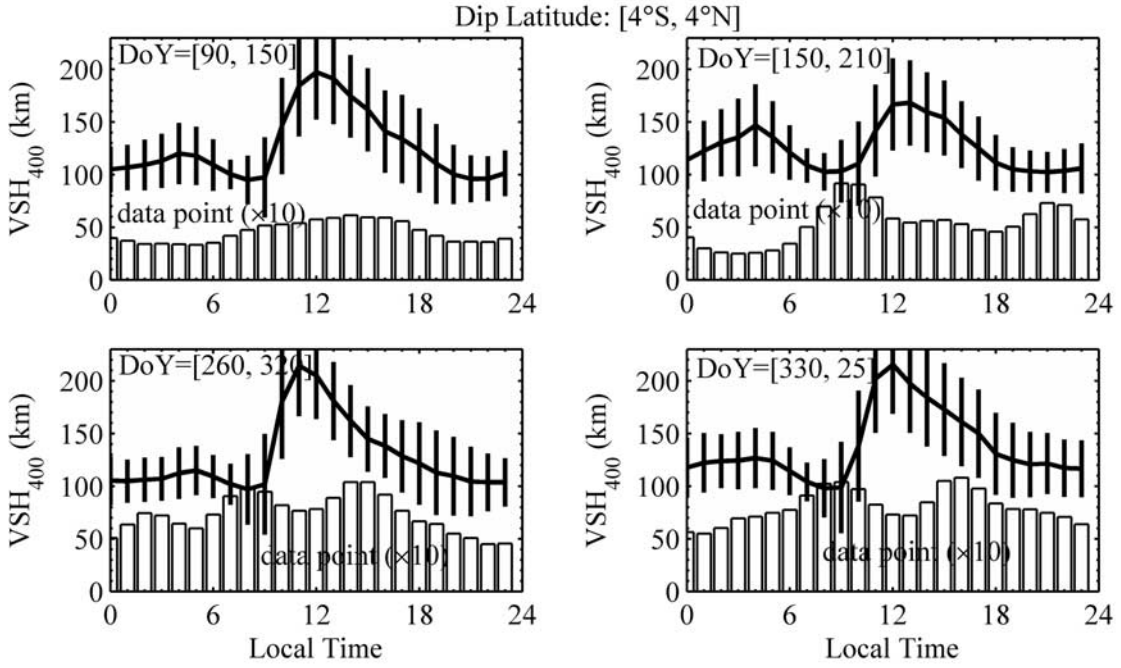

Figure 4a. Local time variation of VSH in four seasons at dip latitude bin [4°S–4°N].

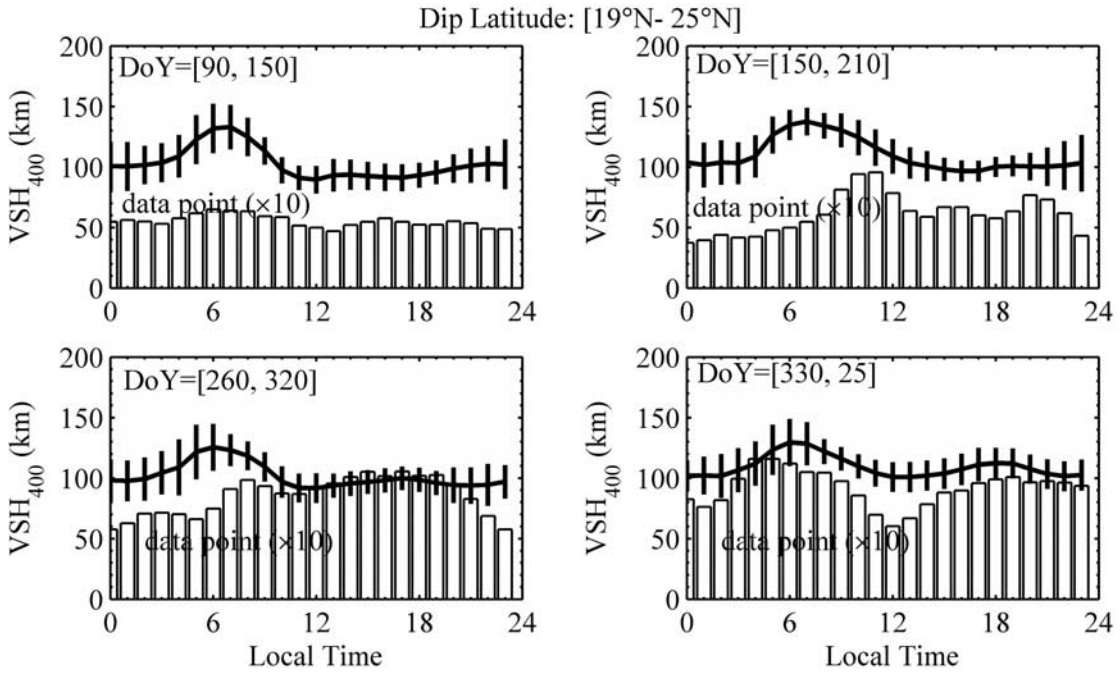

Figure 4b. Local time variation of VSH in four seasons at dip latitude bin [19–25°N].

found in the diurnal pattern of the low latitude VSH_{400}, which seems to be attributed to the morning overshoot in Te [e.g., *Oyama et al.*, 1996; *Sharma et al.*, 2005]. However, the behavior of VSH is not strongly consistent with that of plasma temperature [*Sharma et al.*, 2005; *Zhang et al.*, 2004]. In general, the diurnal variations of VSH_{400} become less distinct in both the northern and southern low latitude in four seasons (take two latitude bins, 19–25°N and 19–25°S, for examples). The daytime values of VSH_{400} are comparable with those at nighttime.

[17] Similar to the conclusion of *Liu et al.* [2007a, 2007b] and *Belehaki et al.* [2006], the VSH values do not follow the diurnal variation pattern of the neutral density-scale height. Further, it should be mentioned that the morning peak in VSH will become more obviously at altitudes higher than 400 km. *Liu et al.* [2007a] revealed that there are two peaks in the diurnal variations of VSH over Arecibo (293.2°E, 18.3°N), one in the early morning and another one located in the afternoon to the evening sector. The VSH discrepancies between the Arecibo ISR and C/F3 observations

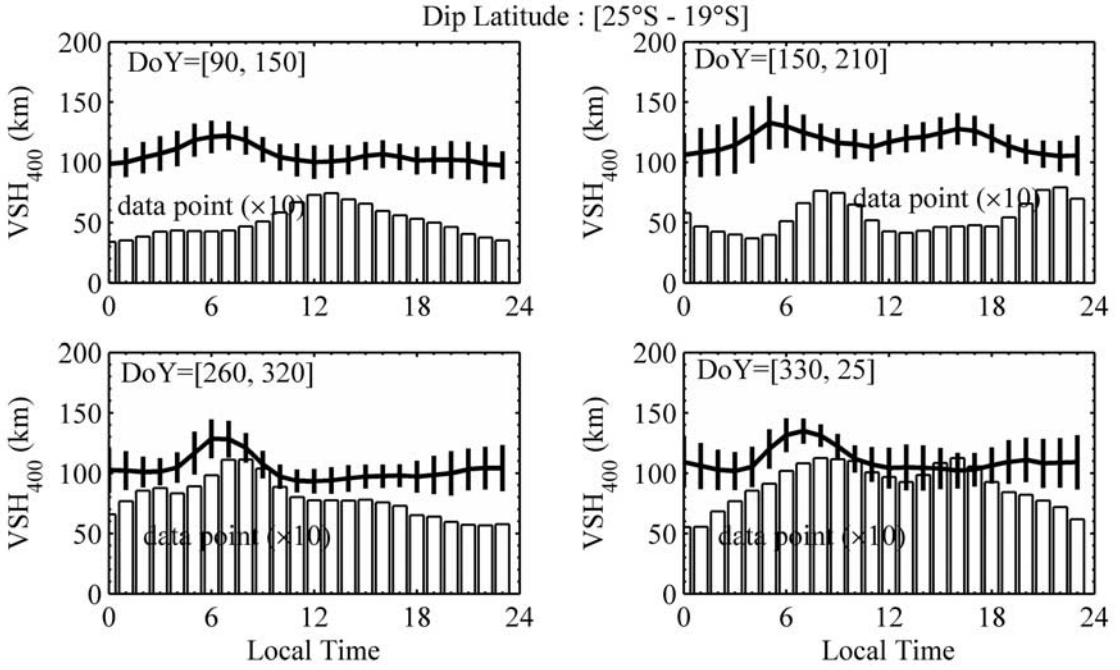

Figure 4c. Local time variation of VSH in four seasons at dip latitude bin [19–25°S].

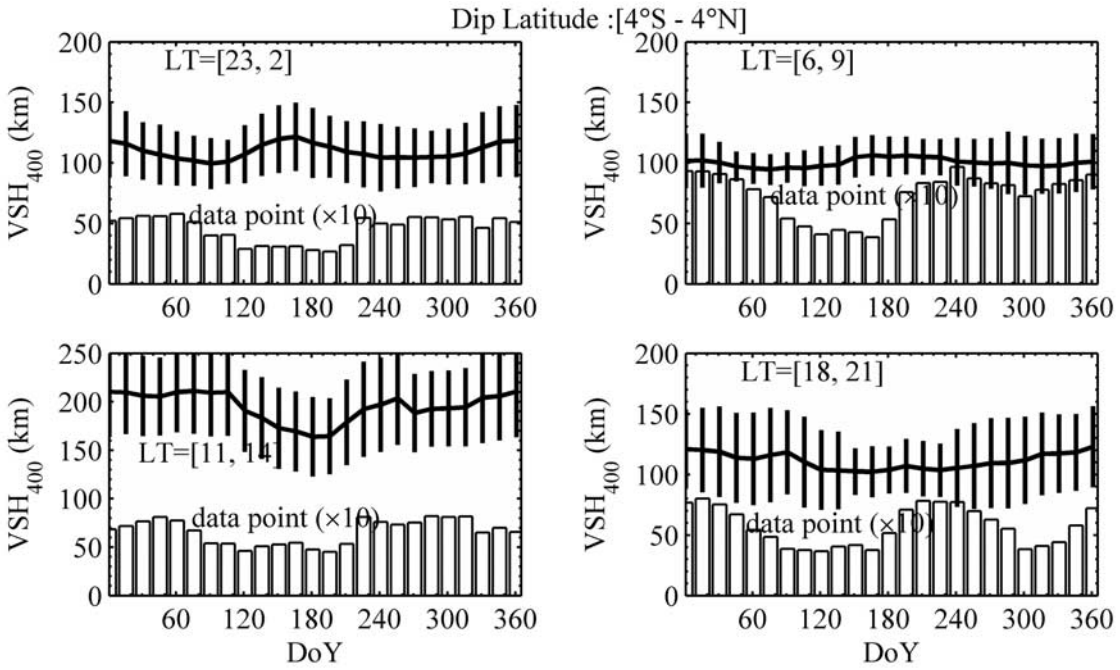

Figure 5a. Seasonal variation of VSH at four local time intervals at dip latitude bin [4°S–4°N].

might be attributed to differences in techniques, epochs and derivations of the VSH. Moreover, *Liu et al.* [2007a] did not take into account the altitudinal dependence of VSH, so their results are not applied at a fixed altitude. In contrast, the present result is fixed at 400 km altitude.

3.2. Seasonal Variation of VSH

[18] Figures 5a–5c shows the median values of VSH_{400} as a function of DOY at dip equator (4°S–4°N dip latitude; Figure 5a), northern low latitude (19–25°N dip latitude; Figure 5b), and southern low latitude (19–25°S dip latitude; Figure 5c). The top plots the results at night and morning, and the bottom plots the results for those during daytime and evening hours.

[19] Around dip equator, as shown in Figure 5a, strong seasonal variations are found in the VSH at daytime and nighttime, while it becomes much weaker during the morning and evening hours. The seasonal dependence of equatorial VSH is generally opposite at daytime and nighttime. The VSH values dominate by an annual component with a

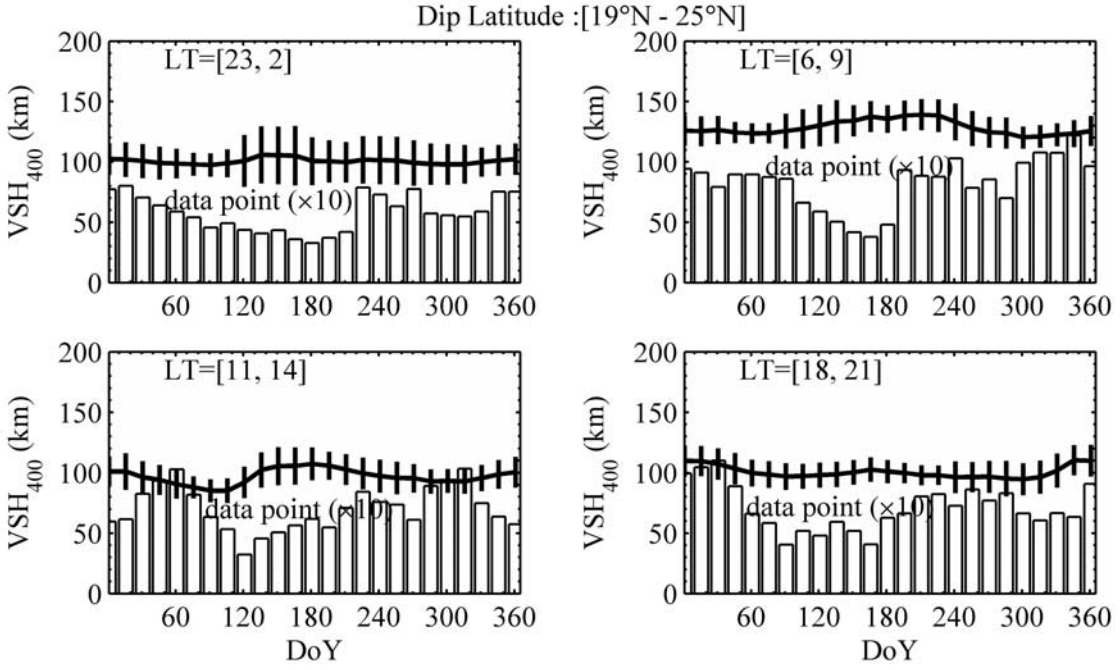

Figure 5b. Seasonal variation of VSH at four local time intervals at dip latitude bin [19–25°N].

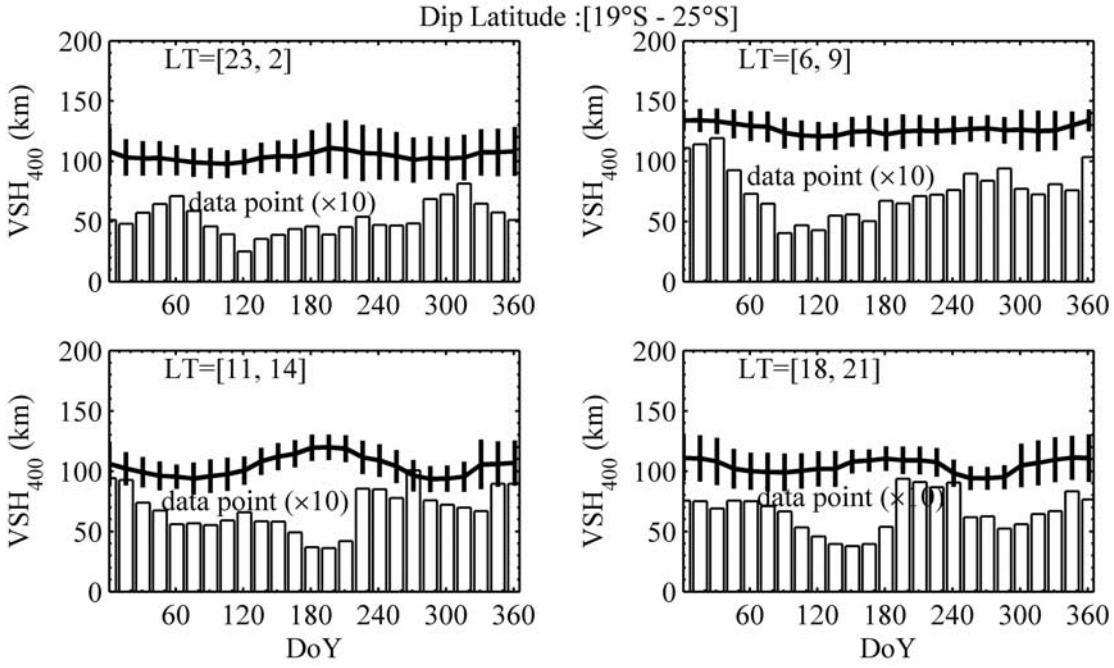

Figure 5c. Seasonal variation of VSH at four local time intervals at dip latitude bin [19–25°S].

maximum at nighttime and a minimum at daytime around DOY 180.

[20] At low latitudes, the seasonal variation of VSH is marked during daytime, with a maximum around DOY 180. A daytime minimum appears around DOY 105 in the northern hemisphere and around DOY 300 in the southern hemisphere. Seasonal differences are also observed in the morning in the northern hemisphere VSH. At rest local times the seasonal variation is less distinct.

[21] For the daytime, the yearly variations of VSH in these three dip latitude bins are consistent with the radio occultation results of *Stankov and Jakowski* [2006b]. However, *Liu et al.* [2006] revealed that a distinct yearly annual variation is presented in global ionogram derived H_m with a maximum in summer during the daytime. The seasonal features in VSH are not as distinct as the ionogram derived H_m over Wuhan and other locations. *Liu et al.* [2007] discussed the physical discrepancies in the behaviors of different scale heights (VSH, H_p and H_m). Moreover, the discrepancies may possibly be attributed to different data sources and different epochs, because the ionogram derived H_m is estimated only from the bottomside profiles while the VSH is deduced from the topside profiles.

3.3. Latitudinal Dependence of VSH

[22] We obtain the latitudinal pattern of VSH by evaluating the median values of VSH_{400} with data points in the given local time, latitude, and DOY windows. Figures 6a–6d shows the latitudinal structure of VSH_{400} in four seasons. In the morning hours (top right), the VSH_{400} tends to decrease at lower latitudes, with a minimum around dip equator. During the nighttime (top left), evening hours (bottom right), and daytime (bottom left), it is also obvious that the VSH decreases with latitude at the higher-latitude part. However, during the nighttime, no major difference was detected for latitudes lower than 40° dip latitude. In contrast, the daytime VSH reaches a huge peak in the equatorial region with two troughs at low latitudes in both hemispheres. This feature is a new finding. The equatorial peak in VSH is also preserved during the evening hours in equinox and winter, but has lower values. Overall, our results reveal the latitudinal behavior of VSH is strongly dependent on local time.

[23] *Stankov and Jakowski* [2006a, 2006b] also made an analysis on the latitudinal behavior of the scale height with the CHAMP IRO observations. They found that the scale height tends to increase at higher latitudes, which is consistent with this analysis. However, as Figure 22 of *Stankov and Jakowski* [2006b] illustrated, the CHAMP VSH has weak latitudinal variations in equinox and summer. Moreover, the equatorial peak only presents in winter daytime CHAMP data, but the minimum is located at 55°S latitude (much higher than that of our results). This discrepancy is possibly related with the difference sample sizes used as well as different solar epochs. As shown above, the equatorial peak in the latitudinal pattern of VSH is most pronounced around local noon. The feature may be smoothed out or become much weaker, if the 0700–1700 LT data are combined together, as *Stankov and Jakowski* [2006b] did.

[24] The cause of the daytime equatorial peak in the latitudinal pattern of VSH is another interesting question. *Liu et al.* [2007a] pointed out that VSH is controlled by many factors, including H_p, vertical drift, and the topside thermal structure. The plasma-scale height will play role in the variations of the VSH, so the first possibility for the increase of equatorial VSH around noon may come from the increase of H_p. This possibility can be discussed with the aid of reported features of Ti at 500 km altitude by *Bhuyan et al.* [2004] and Te at 600 km by *Oyama et al.* [2004]. As they reported, no huge peak can be found in latitudinal dependence of Te and Ti around magnetic equator. If these reported latitudinal features of Te and Ti are similar to that at 400 km, we can exclude the possibility of equatorial VSH

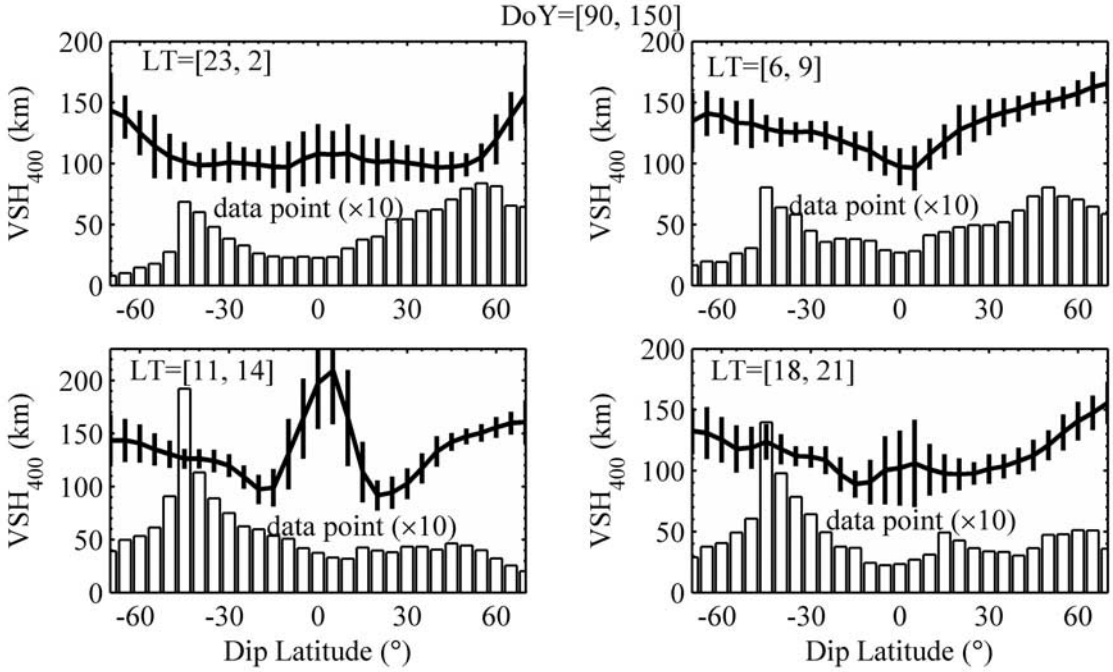

Figure 6a. Latitudinal variation of VSH at four local time intervals in DOY interval [90–150].

peak coming from plasma-scale height. Unfortunately we have no Te and Ti data at altitude 400 km, so we do not know the actual situation for Te and Ti at 400 km. As a result, this possibility needs further investigations.

[25] The second possibility is the daytime effect of the $E \times B$ drift. We know that, the upward plasma drift is induced by daytime equatorial electric fields, which induces the fountain effect playing an important role in the equatorial ionosphere. As a consequence, the peak height is higher around magnetic equator during daytime. We propose the electric field to be a possible candidate to cause the latitudinal behavior of low latitude VSH. However, it requires simulation studies to resolve this issue.

3.4. Longitudinal Pattern of VSH

[26] We obtain the longitudinal behavior of VSH by evaluating the median values of VSH_{400} with data points in the given local time, latitude, longitude, and DOY

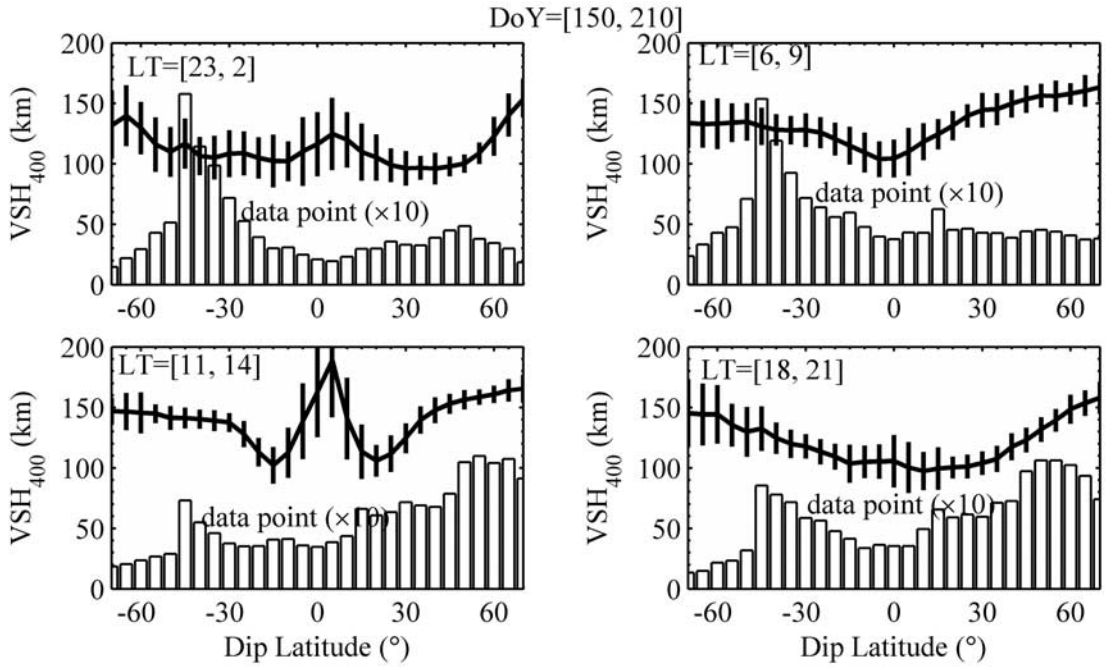

Figure 6b. Latitudinal variation of VSH at four local time intervals in DOY interval [150–210].

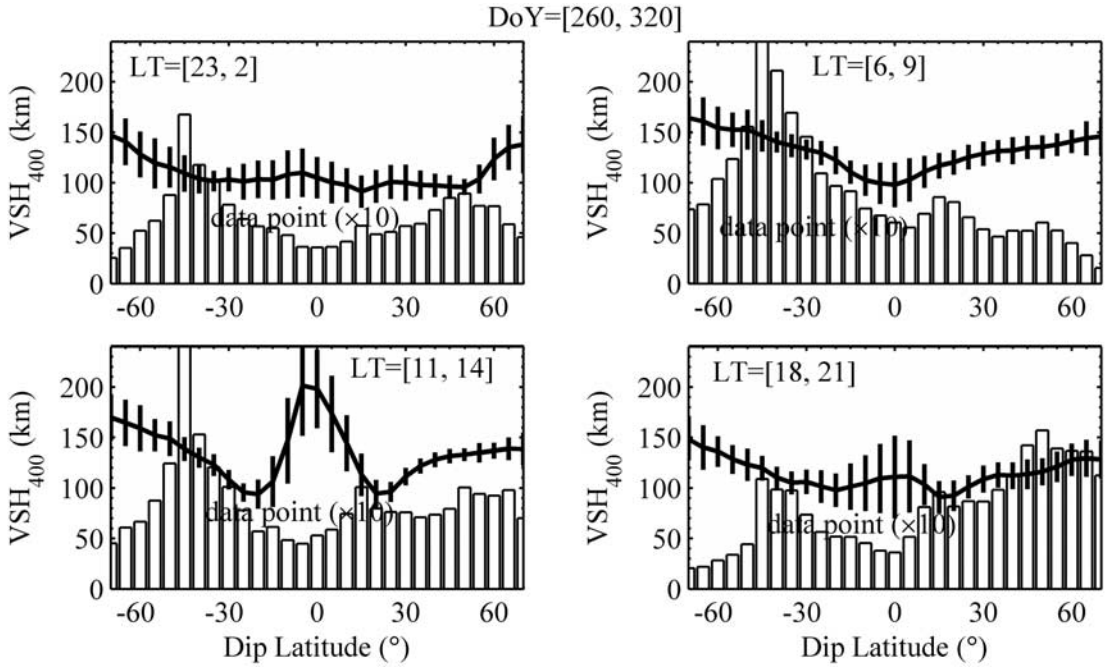

Figure 6c. Latitudinal variation of VSH at four local time intervals in DOY interval [260−320].

windows. Figures 7a −7d plots the longitudinal pattern of VSH_{400} at four local time intervals in four seasons.

[27] From Figures 7a−7d, a complicated longitudinal structure is detected in equatorial VSH_{400}, which is strongly dependent on local time. During the daytime, as illustrated in the bottom left of Figure 7c, the VSH_{400} has a wave-like longitudinal structure. Significant longitudinal variation can also be found in equatorial VSH during July solstice nighttime as well as at local evening sector in equinox and December solstice. Overall, results indicate that complicated structures in the VSH_{400} weaken or disappear at other local time intervals.

[28] Moreover, the longitudinal locations of the equatorial VSH peaks in the DOY interval [260−320] are generally similar to that shown in Figure 2 of *Lin et al.* [2007]. *Lin et al.* [2007] obtained a strong four-peaked longitudinal pattern in the equatorial electron density result with C/F3 observations in September and October 2006. However, their four-peaked longitudinal pattern is most prominent at the EIA crests zones, which is quite different from that of

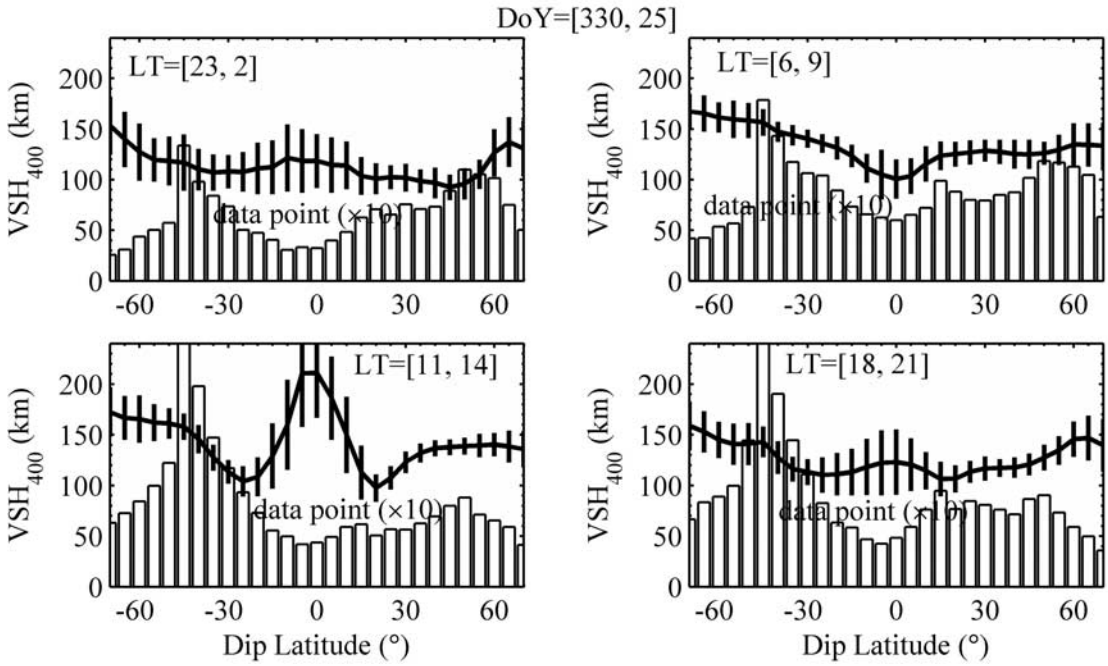

Figure 6d. Latitudinal variation of VSH at four local time intervals in DOY interval [330−25].

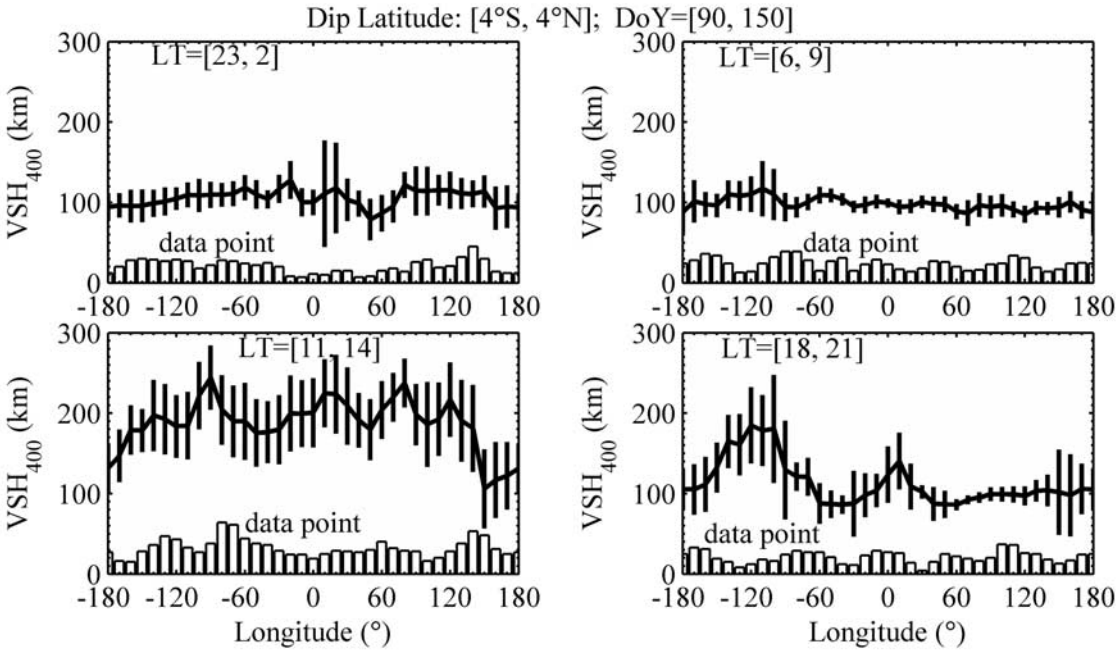

Figure 7a. Longitudinal structure of equatorial VSH at four local time intervals in DOY interval [90–150].

VSH. It is interesting that the wavelike longitudinal structure of VSH gradually disappears when moving from the equatorial region to low latitude, and it is practically absent at equatorial ionization anomaly (EIA) crest and higher latitudes (figures not shown here).

[29] As mentioned before, the longitudinal pattern of VSH is not known yet because of insufficient data coverage. *Kutiev et al.* [2006] could not model the longitude picture of VSH in their model because most of the topside sounder data were clustered around 290°E longitude. *Stankov and Jakowski* [2006a] also made an attempt with the CHAMP IRO observations. They found that there is generally no indication of major longitude differences in H_m (not VSH!). However, it is difficult for us to compare results with each other, because of not only the low number of the CHAMP data, but also the wider latitudinal window their analysis used.

4. Summary

[30] This paper investigates the behaviors of the VSH retrieved from the C/F3 IRO observations in DOY 194 in

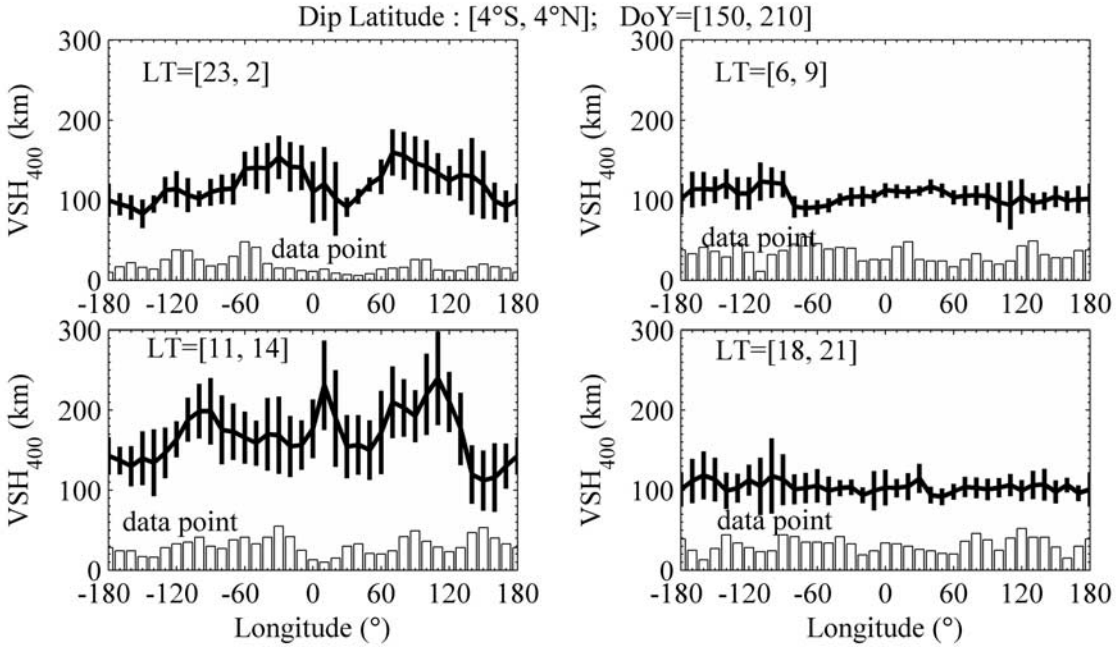

Figure 7b. Longitudinal structure of equatorial VSH at four local time intervals in DOY interval [150–210].

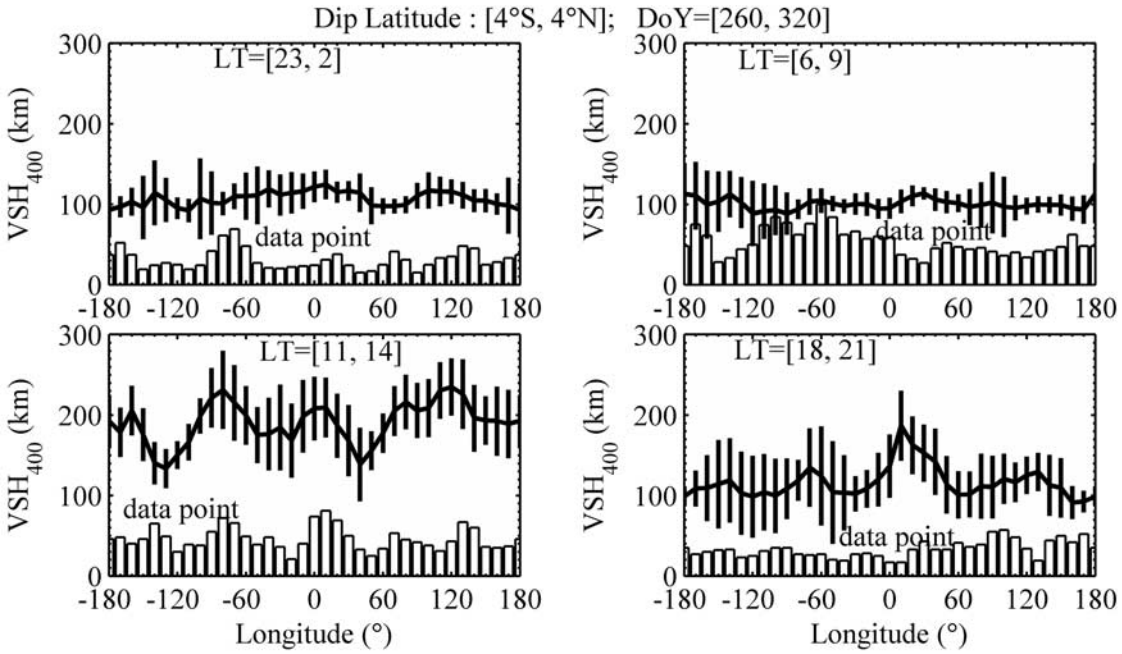

Figure 7c. Longitudinal structure of equatorial VSH at four local time intervals in DOY interval [260–320].

2006 to DOY 60 in 2008. The main results are summarized as follows:

[31] The vertical scale height has marked altitudinal dependence. The VSH at an altitude of 400 km shows appreciable diurnal and seasonal variations. Around dip equator, the daytime VSH are higher, compared to those in the nighttime. In general, there are less distinct diurnal variations of VSH at low latitudes, with a peak around 0600 LT. Strong seasonal variations are found in the equatorial VSH at daytime and nighttime, while it becomes much weaker during the morning and evening hours. Seasonal differences are also observed at low latitudes.

[32] Crucial findings are that this analysis also identifies clear latitudinal and longitudinal behaviors of VSH, which is strongly dependent on local time. The daytime VSH presents a peak in the equatorial region with two troughs at low latitudes. In contrast, no major difference has detected at low latitudes during nighttime. At higher latitudes the

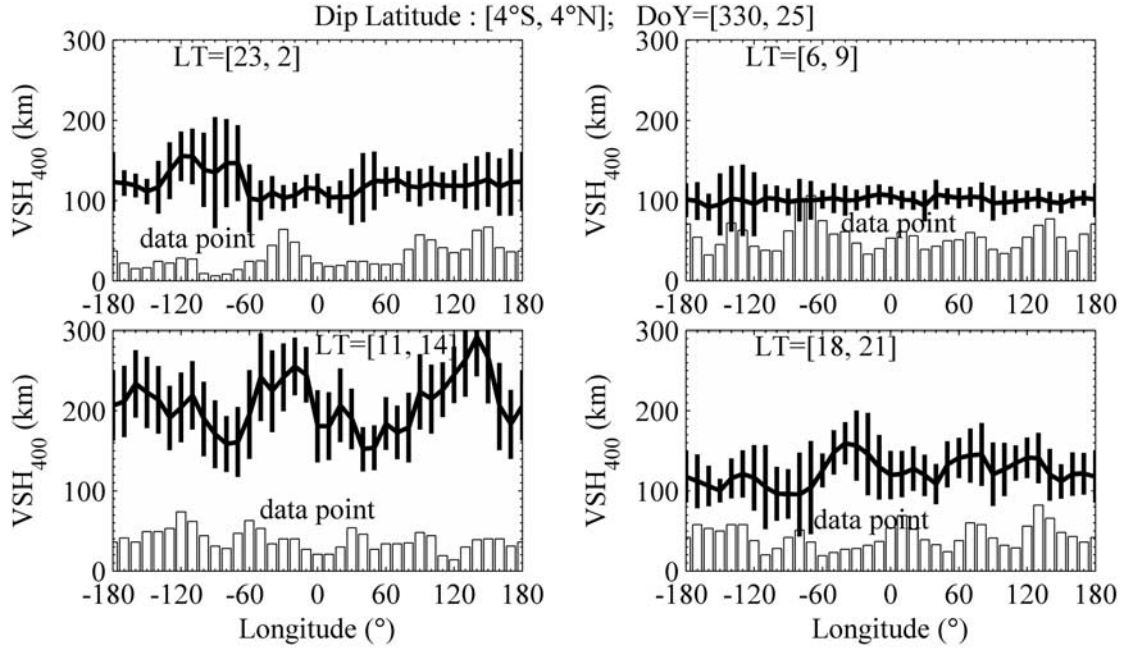

Figure 7d. Longitudinal structure of equatorial VSH at four local time intervals in DOY interval [330–25].

VSH tends to increase with latitude. An outstanding feature of VSH is the complicated longitudinal pattern of daytime VSH. There are significant wave-like longitudinal variations in equatorial VSH during daytime, while it becomes weaker or disappears at other local time intervals. This is a crucial finding. In contrast, the longitudinal variations of VSH become not remarkable during both daytime and nighttime at low and middle latitudes. Further, this investigation confirms that the VSH is not so tightly correlated with the neutral or plasma-scale heights [*Liu et al.*, 2007a, 2007b].

[33] **Acknowledgments.** The authors would like to thank two reviewers for their kindly and valuable suggestions. This study made use of IRO data from the COSMIC Data Analysis and Archive Center (CDAAC). This research was supported by National Natural Science Foundation of China (40725014, 40674090, and 40636032) and National Important Basic Research Project (2006CB806306).

[34] Wolfgang Baumjohann thanks Jan Lastovicka and Shigeto Watanabe for their assistance in evaluating this paper.

References

Belehaki, A., P. Marinov, I. Kutiev, N. Jakowski, and S. Stankov (2006), Comparison of the topside ionosphere scale height determined by topside sounders model and bottomside Digisonde profiles, *Adv. Space Res.*, *37*, 963–966, doi:10.1016/j.asr.2005.09.014.

Bhuyan, P. K., M. Chamua, P. Subrahmanyam, and S. C. Garg (2004), Diurnal, seasonal and latitudinal variations of ion temperature measured by the SROSS C2 satellite in the Indian zone equatorial and low latitude ionosphere and comparison with the IRI, *J. Atmos. Sol. Terr. Phys.*, *66*(3–4), 301–312, doi:10.1016/j.jastp.2003.12.002.

Bilitza, D. (2001), International reference ionosphere 2000, *Radio Sci.*, *36*(2), 261–275, doi:10.1029/2000RS002432.

Bilitza, D., B. W. Reinisch, S. M. Radicella, S. Pulinets, T. Gulyaeva, and L. Triskova (2006), Improvements of the international reference ionosphere model for the topside electron density profile, *Radio Sci.*, *41*, RS5S15, doi:10.1029/2005RS003370.

Booker, H. G. (1977), Fitting of multi-region ionospheric profiles of electron density by a single analytic function of height, *J. Atmos. Terr. Phys.*, *39*, 619–623, doi:10.1016/0021-9169(77)90072-1.

Depuev, V. H., and S. A. Pulinets (2004), A global empirical model of the ionospheric topside electron density, *Adv. Space Res.*, *34*(9), 2016–2020, doi:10.1016/j.asr.2004.05.006.

Di Giovanni, G., and S. M. Radicella (1990), An analytical model of the electron density profile in the ionosphere, *Adv. Space Res.*, *10*(11), 27–30, doi:10.1016/0273-1177(90)90301-F.

Hajj, G. A., C. O. Ao, B. A. Iijima, D. Kuang, E. R. Kursinski, A. J. Mannucci, T. K. Meehan, L. J. Romans, M. de la Torre Juarez, and T. P. Tunck (2004), CHAMP and SAC-C atmospheric occultation results and intercomparisons, *J. Geophys. Res.*, *109*, D06109, doi:10.1029/2003JD003909.

Huang, X., and B. W. Reinisch (1996), Vertical electron profiles from the Digisonde network, *Adv. Space Res.*, *18*(6), 121–129, doi:10.1016/0273-1177(95)00912-4.

Huang, X., and B. W. Reinisch (2001), Vertical electron content from ionograms in real time, *Radio Sci.*, *36*(2), 335–342, doi:10.1029/1999RS002409.

Jakowski, N., A. Wehrenpfennig, S. Heise, C. Reigber, H. Lühr, L. Grunwaldt, and T. K. Meehan (2002), GPS radio occultation measurements of the ionosphere from CHAMP: Early results, *Geophys. Res. Lett.*, *29*(10), 1457, doi:10.1029/2001GL014364.

Kutiev, I. S., P. G. Marinov, and S. Watanabe (2006), Model of topside ionosphere scale height based on topside sounder data, *Adv. Space Res.*, *37*, 943–950, doi:10.1016/j.asr.2005.11.021.

Lee, C.-C., and B. W. Reinisch (2007), Quiet-condition variations in the scale height at F2-layer peak at Jicamarca during solar minimum and maximum, *Ann. Geophys.*, *25*(12), 2541–2550.

Lei, J., L. Liu, W. Wan, and S.-R. Zhang (2005), Variations of electron density based on long-term incoherent scatter radar and ionosonde measurements over Millstone Hill, *Radio Sci.*, *40*, RS2008, doi:10.1029/2004RS003106.

Lei, J., et al. (2007), Comparison of COSMIC ionospheric measurements with ground-based observations and model predictions: Preliminary results, *J. Geophys. Res.*, *112*, A07308, doi:10.1029/2006JA012240.

Lin, C. H., C. C. Hsiao, J. Y. Liu, and C. H. Liu (2007), Longitudinal structure of the equatorial ionosphere: Time evolution of the four-peaked EIA structure, *J. Geophys. Res.*, *112*, A12305, doi:10.1029/2007JA012455.

Liu, H., C. Stolle, S. Watanabe, T. Abe, M. Rother, and D. L. Cooke (2007), Evaluation of the IRI model using CHAMP observations in polar and equatorial regions, *Adv. Space Res.*, *39*(5), 904–909, doi:10.1016/j.asr.2006.08.006.

Liu, L., W. Wan, and B. Ning (2006), A study of the ionogram derived effective scale height around the ionospheric h_mF_2, *Ann. Geophys.*, *24*(3), 851–860.

Liu, L., H. Le, W. Wan, M. P. Sulzer, J. Lei, and M.-L. Zhang (2007a), An analysis of the scale heights in the lower topside ionosphere based on the Arecibo incoherent scatter radar measurements, *J. Geophys. Res.*, *112*, A06307, doi:10.1029/2007JA012250.

Liu, L., W. Wan, M.-L. Zhang, B. Ning, S.-R. Zhang, and J. M. Holt (2007b), Variations of topside ionospheric scale heights over Millstone Hill during the 30-day incoherent scatter radar experiment, *Ann. Geophys.*, *25*, 2019–2027.

Luan, X., L. Liu, W. Wan, J. Lei, S.-R. Zhang, J. M. Holt, and M. P. Sulzer (2006), A study of the shape of the topside electron density profile derived from incoherent scatter radar measurements over Arecibo and Millstone Hill, *Radio Sci.*, *41*, RS4006, doi:10.1029/2005RS003367.

Nambala, F.-J., L.-A. McKinnell, and E. Oyeyemi (2008), Variations in the ionospheric scale height parameter at the F2 peak over Grahamstown, South Africa, *Adv. Space Res.*, *42*, 707–711, doi:10.1016/j.asr.2007.10.030.

Oyama, K.-I., S. Watanabe, Y. Su, T. Takahashi, and K. Hiro (1996), Seasonal, local time, and longitudinal variations of electron temperature at the height of ~600 km in the low latitude region, *Adv. Space Res.*, *18*(6), 269–278, doi:10.1016/0273-1177(95)00936-1.

Oyama, K.-I., P. Marinov, I. Kutiev, and S. Watanabe (2004), Low latitude model of Te at 600 km based on Hinotori satellite data, *Adv. Space Res.*, *34*(9), 2004–2009, doi:10.1016/j.asr.2004.07.013.

Rawer, K. (1988), Synthesis of ionospheric electron density profiles with Epstein functions, *Adv. Space Res.*, *8*(4), 191–198, doi:10.1016/0273-1177(88)90239-6.

Rawer, K., D. Bilitza, and T. L. Gulyaeva (1985), New formulas for IRI electron density profile in the topside and middle ionosphere, *Adv. Space Res.*, *5*(7), 3–12, doi:10.1016/0273-1177(85)90347-3.

Reinisch, B. W., and X. Huang (2001), Deducing topside profiles and total electron content from bottomside ionograms, *Adv. Space Res.*, *27*(1), 23–30, doi:10.1016/S0273-1177(00)00136-8.

Reinisch, B. W., X. Huang, A. Belehaki, J. Shi, M. Zhang, and R. Ilma (2004), Modeling the IRI topside profile using scale height from ground-based ionosonde measurements, *Adv. Space Res.*, *34*, 2026–2031, doi:10.1016/j.asr.2004.06.012.

Rocken, C., Y.-H. Kuo, W. Schreiner, D. Hunt, S. Sokolovskiy, and C. McCormick (2000), COSMIC system description, *Terr. Atmos. Oceanic Sci.*, *11*, 21–52.

Schreiner, W., C. Rocken, S. Sokolovskiy, S. Syndergaard, and D. Hunt (2007), Estimates of the precision of GPS radio occulations from the COSMIC/FORMOSAT-3 mission, *Geophys. Res. Lett.*, *34*, L04808, doi:10.1029/2006GL027557.

Sharma, D. K., J. Rai, M. Israil, and P. Subrahmanyam (2005), Diurnal, seasonal and longitudinal variations of ionospheric temperatures of the topside F region over the Indian region during solar minimum (1995–1996), *J. Atmos. Sol. Terr. Phys.*, *67*, 269–274, doi:10.1016/j.jastp.2004.09.004.

Stankov, S. M., and N. Jakowski (2006a), Topside plasma scale height retrieved from radio occultation measurements, *Adv. Space Res.*, *37*, 958–962, doi:10.1016/j.asr.2005.12.009.

Stankov, S. M., and N. Jakowski (2006b), Topside ionospheric scale height analysis and modeling based on radio occultation measurements, *J. Atmos. Sol. Terr. Phys.*, *68*, 134–162, doi:10.1016/j.jastp.2005.10.003.

Stankov, S. M., N. Jakowski, S. Heise, P. Muhtarov, I. Kutiev, and R. Warnant (2003), A new method for reconstruction of the vertical electron density distribution in the upper ionosphere and plasmasphere, *J. Geophys. Res.*, *108*(A5), 1164, doi:10.1029/2002JA009570.

Zhang, M.-L., B. W. Reinisch, J. S. Shi, S. Wu, and X. Wang (2006), Diurnal and seasonal variation of the ionogram-derived scale height at the F2 peak, *Adv. Space Res.*, *37*, 967–971, doi:10.1016/j.asr.2006.02.004.

Zhang, S.-R., J. M. Holt, A. M. Zalucha, and C. Amory-Mazaudier (2004), Midlatitude ionospheric plasma temperature climatology and empirical model based on Saint Santin incoherent scatter radar data from 1966 to 1987, *J. Geophys. Res.*, *109*, A11311, doi:10.1029/2004JA010709.

M. He, L. Liu, W. Wan, and M.-L. Zhang, Beijing National Observatory of Space Environment, Institute of Geology and Geophysics, Chinese Academy of Sciences, Beijing 100029, China. (liul@mail.igcas.ac.cn)